Applied Surface Science 565 (2021) 150608

Contents lists available at ScienceDirect

Applied Surface Science

journal homepage: www.elsevier.com/locate/apsusc

Full Length Article

Influence of electrolyte selection on performance of tantalum anodic oxide memristors

Ivana Zrinski [a], Alexey Minenkov [b], Cezarina Cela Mardare [a,c], Jan Philipp Kollender [a,d], Shaukat Ali Lone [a], Achim Walter Hassel [a,c], Andrei Ionut Mardare [a,*]

[a] Institute of Chemical Technology of Inorganic Materials, Johannes Kepler University Linz, Altenberger Str. 69, 4040 Linz, Austria
[b] Christian Doppler Laboratory for Nanoscale Phase Transformations, Center for Surface and Nanoanalytics, Johannes Kepler University Linz, Altenberger Str. 69, 4040 Linz, Austria
[c] Danube Private University, Steiner Landstrasse 124, 3500 Krems-Stein, Austria
[d] EMPA, Laboratory for Joining Technologies & Corrosion, Swiss Federal Laboratories for Materials Science and Technology, Überlandstrasse 129, 8600 Dübendorf, Switzerland

ARTICLE INFO

Keywords:
Memristor
Anodic oxide
Tantalum oxide
Valve metals

ABSTRACT

Anodic memristors obtained by electrochemical anodization of Ta in phosphate, borate and citrate buffer solutions are studied. Memristive behaviour is demonstrated by electrical switching between high and low conductive states. The endurance and retention of devices are analysed. The use of phosphate leads to 4 switching levels and the highest ratio between high and low resistive states. All studied oxides are stoichiometric Ta_2O_5 and only P is detected inside anodic memristors. The improved memristive characteristics of oxides anodized in phosphate are attributed to an increase of O vacancies due to the presence of Ta oxyphosphate, which is believed to mediate spatial pinning of conductive filaments positions during read/write. The anodic memristors show high stability, enhanced endurance and retention that combined with their active layer low fabrication cost makes them ideal candidates for industrial implementation.

1. Introduction

Tantalum oxide-based memristors fabricated in a metal-insulator-metal (MIM) geometry, with Ta bottom electrode, Ta_2O_5 active layer and Pt top electrode have multiple applications. They are essential in Resistive Random Access Memory (ReRAM) [1–3], sensors [4] or as building blocks for neural networks and neuromorphic applications [3,5,6]. The electrically induced resistive switching mechanism, between a high resistive state (HRS) and a low resistive state (LRS), is based on field and temperature-assisted ion migration. This leads to the formation of conductive paths in the insulating oxide layer, which coupled with local redox processes result in an overall resistance change [7]. The reduction reaction is responsible for the formation of a conductive filament (CF) connecting both metallic electrodes, while its partial re-oxidation increases the device resistance. Switching from the usually insulating HRS (OFF or RESET state) to the conductive LRS (ON or SET state) is assumed to be done by movement of O vacancies within the filament by a direct contribution of mobile cations and additional O vacancies forming the CFs in high electric fields [8,9]. The nature of the Ta_2O_5 regarded as a solid electrolyte in memristive devices strongly depends on the fabrication route. Even though most studies focus on sputtered Ta_2O_5 [3,10,11,44] due to high film quality and reproducibility, the anodic formation of metallic oxides recently started to be explored as a prominent approach for industrial implementation [12,13]. However, the deposition by sputtering remains an excellent choice for the production of metallic bottom and top electrodes, such as Ta and Pt, in memristive devices. The memristive function is defined by the oxide (active) layer and its anodic formation may offer additional tuning parameters, thus enlarging the range of possible fabrication methods [14]. The main motivation of anodization is the use of a simpler and easier controllable fabrication technique, as an alternative to sputtering, atomic layer deposition and similar methods that require more complex processing parameters control [15–17].

The current work focuses on the use of electrochemically grown Ta_2O_5 for anodic memristors fabrication. The reported Ti, Hf/Nb and Ta-based anodic memristors [18–20] reached endurances up to 4500, 10^3 and 10^6 cycles, respectively, while retention times up to 10^4 s were specified for Ta anodic memristors. Moreover, memristors based on

* Corresponding author.
E-mail address: Andrei.mardare@jku.at (A.I. Mardare).

https://doi.org/10.1016/j.apsusc.2021.150608
Received 16 March 2021; Received in revised form 30 June 2021; Accepted 8 July 2021
Available online 10 July 2021
0169-4332/© 2021 The Author(s). Published by Elsevier B.V. This is an open access article under the CC BY license (http://creativecommons.org/licenses/by/4.0/).

anodic Ta_2O_5 showed multi-level switching, which promises superior application properties. However, the effect of different electrolytes on the performance characteristics of Ta_2O_5 memristors is still far from a brimming comprehension. Properties of the anodic oxide films (thickness, morphology, chemical and structural composition) are tuned by controlling the process parameters (voltage, anodizing time and electrolyte composition) [21–23]. Thus, the number of oxygen vacancies and cation contribution may vary with the use of different electrolytes, leading to the formation of CFs with different sizes and shapes at different positions within the active layer [24,25]. In this way, the electrical properties may be strongly affected and the electrolyte selection may become highly relevant for industrial implementation. Finally, the goal was to find the optimal conditions for the fabrication of the insulating layer, in which CFs could form at constant positions improving the stability of memristive devices.

For these reasons, in the frame of the current investigation, Ta metallic thin films are electrochemically anodized in phosphate, citrate and borate buffer electrolytes. Incorporation of citrate anion, phosphate and borate ions in anodic oxide layers were previously reported with significant effects on their characteristics [21,26,27]. Additionally, potentiodynamic anodization at varying rates of potential increase was designed here specifically for testing the electrolyte incorporation effect on memristive properties of Ta_2O_5.

2. Experimental section

2.1. Fabrication of anodic Ta oxide memristors

Metallic Ta thin films were deposited by sputtering using an ultra-high vacuum system (Mantis Deposition, United Kingdom) with a base pressure in the range of 10^{-6} Pa. Tantalum thin films with a thickness of approximately 300 nm were deposited on thermally pre-oxidized Si wafers at 950 °C from a high purity Ta target (99.95% Demaco, The Netherlands). The Ta film deposition was performed at room temperature in Ar atmosphere with a pressure of $5 \cdot 10^{-1}$ Pa using DC power of 80 W. For ensuring thickness uniformity, the substrate was rotated at 5 rpm during deposition.

Following the Ta film deposition, the substrates were electrochemically anodized at ambient conditions in three different electrolytes: phosphate buffer (PB), borate buffer (BB), and citrate buffer (CB) solutions. In order to prepare buffer solutions, standard protocols were followed [28]. The detailed information about reagents used for the buffer preparation is given in the supplementary materials. Anodic oxide growth was carried out potentiodynamically at 10 mV s^{-1}, 100 mV s^{-1}, and 1000 mV s^{-1}. The cyclic voltammograms were recorded for two groups of samples, by driving the potentials up to 4 V or 8 V (*vs.* standard hydrogen electrode SHE) and back to 0 V using each of the buffered solutions. A CompactStat potentiostat (Ivium Technologies, The Netherlands) connected to a three-electrode cell was employed in this process, in which a graphite foil 0.5 mm thick (99.8% ThermoFisher, Germany) served as counter electrode, a Hg/Hg_2SO_4/sat. K_2SO_4 electrode (0 V *vs.* $Hg/Hg_2SO_4 = 0.640$ V *vs.* SHE) as reference electrode and Ta thin film as the working electrode.

Following the anodic oxide formation on Ta, the samples were brought back into vacuum for top electrode patterning using a 30 μm thick Ni shadow mask foil (Mecachimique, France) placed in intimate contact with the Ta_2O_5 surface. The fabrication of the memristive devices was finalized by sputtering 100 nm thick Pt electrodes (200 μm in diameter) from a high purity target (99.95%, MaTeck, Germany). in Ar atmosphere (50 W, $5 \cdot 10^{-1}$ Pa) at room temperature. Following this procedure, the emerging memristive devices have Ta as the bottom electrode, Pt as the top electrode and Ta_2O_5 as solid electrolyte sandwiched between the two metallic electrodes.

2.2. Electrical characterization

Electrical measurements were performed using a Keithely 2450 SourceMeter Unit (SMU) connected to a Gantry robot developed in-house. The robot itself containing high precision XYZ translation stages is equipped with two microscope cameras (Bresser, Germany) for allowing top (normal) and side (45° angle) viewing of the Pt electrodes to be contacted. A force sensor attached to the Z stage holds a W needle with a tip diameter of 10 μm used for soft contacting the top electrode of the measured memristor. This occurs while keeping the force at a constant value of 20 ± 2 mN. The bottom metallic film was contacted by a stainless steel needle in hard contact to the Ta thin film at the edge of the Si wafer. The whole system was controlled by LabView® software self-developed for performing current-voltage (*I-U*) sweeps, endurance and retention tests. All experiments were performed in ambient conditions (22 °C, 55% RH) and the voltage was applied to the Ta bottom electrode while the top Pt electrode was grounded. Using the SMU, *I–U* sweeps were recorded with the compliance current being controlled in the mA range, depending on the fabrication conditions of the memristors (supporting electrolyte, oxide thickness). Endurance and retention tests were done up to 10^6 cycles by biasing first the memristors at their voltages corresponding to switching between the LRS and HRS (U_{set} and U_{reset}) with a frequency of 260 Hz. The device resistance was always read by applying a voltage of 0.1 V. The values of U_{set} and U_{reset} ranged between ±0.5 and ±2.0 V.

2.3. Imaging and analysis techniques

High resolution and scanning transmission electron microscopy investigation (HRTEM, STEM) of memristors cross-sections was performed via JEOL JEM-2200FS (JEOL, Japan) equipped with in-column Ω-filter and operated at 200 kV acceleration voltage. Specimens were prepared by focused ion beam (FIB) milling using a Zeiss Crossbeam 1540XB (ZEISS, Germany). Element characterization of specimens was done in STEM mode by energy-dispersive X-ray spectroscopy (EDX) using the detector from Oxford Instruments (UK) and dedicated Aztec software. (HR)TEM data analysis was done with Gatan Microscopy Suite and JEMS simulation software. In order to investigate the chemical composition of the Ta oxide thin films, X-ray photoelectron spectroscopy (XPS) measurements were conducted on all oxides produced by anodization in various electrolytes. The system employed for these investigations was a ThetaProbe XPS system (Thermo Scientific, UK) using a monochromated Al K_α X-ray source (1486.6 eV). The spot size was 400 μm in diameter. Survey spectra were acquired with a pass energy of 200 eV and a binding energy step of 1 eV, whereas for the high-resolution spectra, pass energy of 20 eV with an energy step of 0.05 eV were used. A dual flood gun was used to compensate for charges accumulated on the surface. When sputtering for surface cleaning was performed, a 2 × 2 mm^2 spot was bombarded for 10 s with Ar^+ ions, leading to the removal of surface layer contamination. The measured spectra were corrected with respect to C1s peak coming from adventitious carbon and considered to have a binding energy of 285.0 eV. The spectra were evaluated using the Avantage software package from the manufacturer of the XPS equipment.

3. Results and discussion

3.1. Anodic memristor structure and composition

Throughout this study, all memristive devices analysed have a straightforward MIM structure defined by superimposed $Pt/Ta_2O_5/Ta$ layers. A schematic description of the experimental arrangement is presented in Fig. 1(a) where the position of the electrical contacts and the measurement strategy is described. In Fig. 1(b) several top electrodes are imaged by SEM allowing an accurate observation. One can see well-defined Pt top electrodes and no diffuse edges or distorted shapes

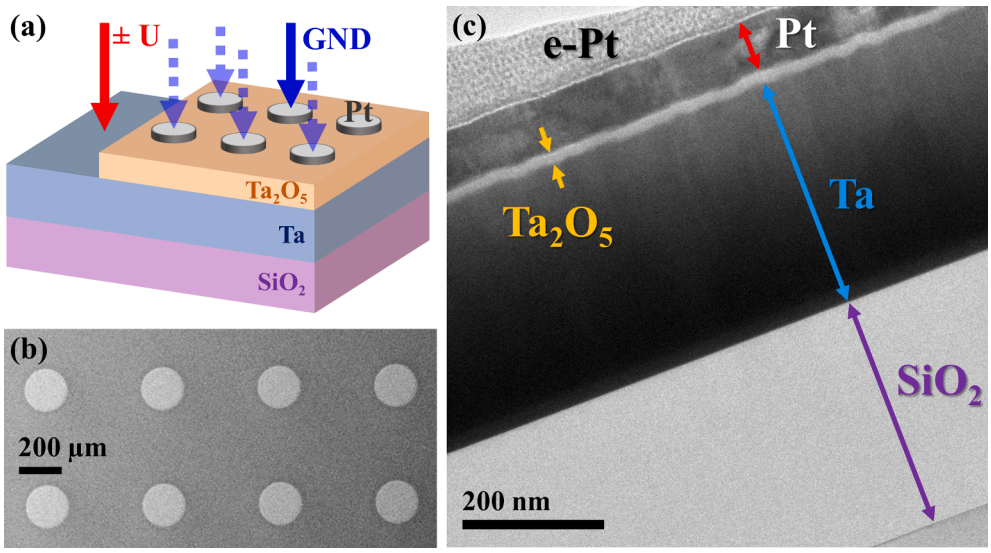

Fig. 1. (a) Experimental arrangement for memristive testing, (b) SEM top-view image of the electrodes, (c) snapshot of the TEM lamella, e-Pt corresponds to the FIB capping layer.

could be found. This emphasizes that high electrode reproducibility is possible by using affordable thin shadow masks in applications where the extra chemical treatment of surfaces (*i.e.* during lithographic processes) is undesirable. Additional images of top electrodes and memristor cross-section structure are presented in supplemental Fig. S1.

Unfortunately, the typical resolution of SEM is unsatisfactory for a closer observation of the anodic ultrathin oxide film [29]. Utilizing TEM imaging of the entire memristor device (Fig. 1(c)) one can observe no cracks, voids, or mechanic failures of any kind neither at the interfaces nor within the layers. From microstructural point of view, all memristive devices analysed in this work are robust, adherent to the substrate, and no mechanical defects at interfaces were observed.

The chemical composition of the anodic oxides under study is relevant for concluding upon the effect of electrolyte incorporation on final memristive behaviour. In Fig. 2 cross-section STEM-EDX image of an anodic memristor (for the case of PB electrolyte) is presented. In part (a) of the figure the high-angle annular dark-field (HAADF) STEM image and corresponding EDX mappings are provided. The location of Pt, O and Ta clearly depicts the nano-scale morphology of the anodic memristor with a well-defined anodic oxide layer sandwiched between Pt (top) and Ta (bottom) electrodes. The possibility of electrolyte species trapped inside the oxide during anodization was also explored here. Unfortunately, the resolution of EDX was not sufficient to distinguish electrolyte incorporation reliably. A small-area EDX measurement was performed in the region of the anodic oxide and the results are presented in Fig. 2(b) together with the corresponding map sum spectrum. It is

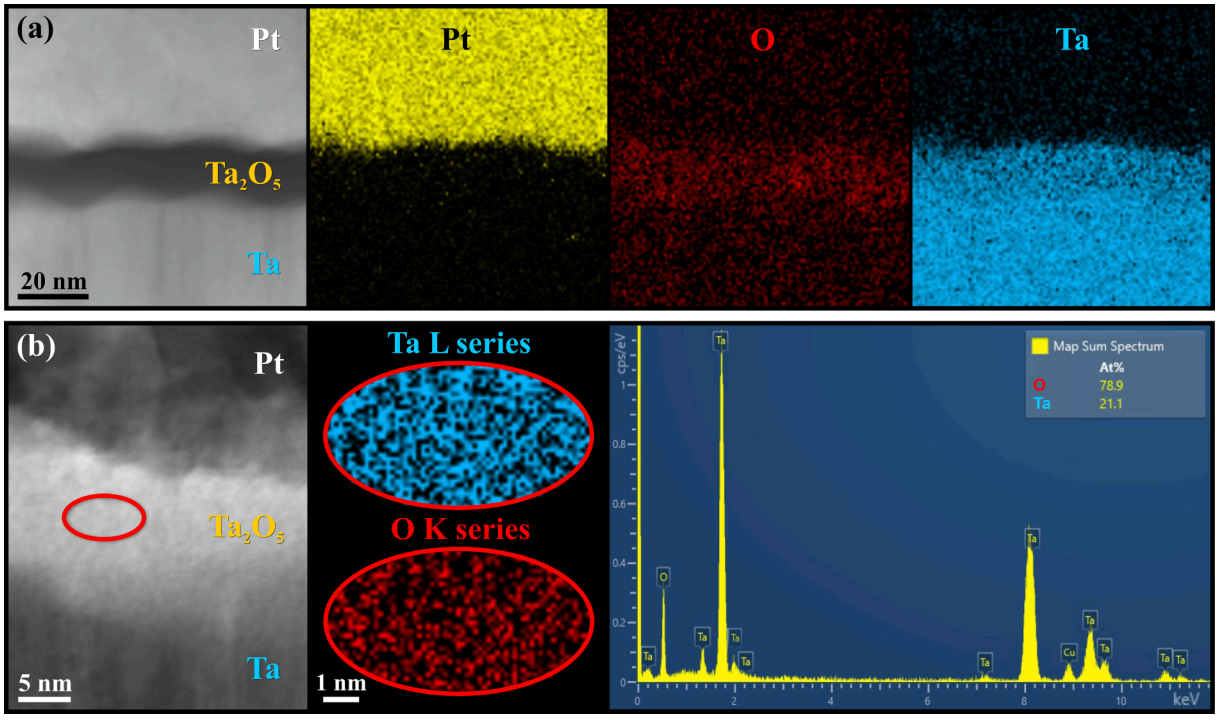

Fig. 2. (a) HAADF STEM image and EDX cross-section mapping of the typical anodic memristor grown in PB at 8 V, 100 mV s^{-1}, (b) bright-field (BF) STEM image and EDX measurement in the anodic oxide layer area together with corresponding map sum spectrum. The Cu peaks correspond to the TEM grid.

worth mentioning though that the EDX peak corresponding to P (K series) strongly overlaps with the Pt (M series) peak, making its recognition in the memristor grown in PB practically impossible. However, one can estimate the Ta/O atoms ratio in the oxide layer. This assessment (±3 at.%) shown in part (b) of Fig. 2 together with colour-coded compositional mappings of Ta and O gives roughly 21 at.% of Ta in the anodic oxide. Nevertheless, additional oxidation of the lamella during transfer to TEM is possible and should not be excluded. Thus, one can see also the minor presence of O in the Pt and Ta layers (Fig. 2(a)).

Since STEM-EDX can only provide a qualitative chemical analysis of anodic memristors on Ta (as exemplified in Fig. 2), XPS was performed for all memristors before Pt top electrode deposition to make a step towards in-detail quantitative analysis. The relevant XPS spectra are shown in Fig. 3(a–c) as measured in oxides grown in various electrolytes. The surface surveys show the various peaks of Ta, O, C, and Na. A small amount of Na (<1.5 at.%) was detected in all memristors due to its presence in all electrolytes used for the formation of the Ta oxide layer. Traces of Zn (<0.6 at.%) were as well detected on samples grown in CB and PB, and they were attributed to trace impurity found in the precursors used for the electrolytes production. The C peaks (C 1s and C KLL Auger peak) are generated by the adventitious carbon adsorbed from the environment (as was evidenced by the peaks disappearance after a short sputtering cleaning process).

For the anodic oxide grown in BB (part (a) of Fig. 3), no peak belonging to B (binding energy for B 1s at 187.3 eV) could be found. This indicates the absence or extremely low amounts of B species incorporation from the electrolyte into the Ta oxide film. This conclusion was confirmed by high-resolution spectra acquired between 180.3 and 196.3 eV, where also no peak was visible. The literature reports about the incorporation of B^{3+} ions from the electrolyte at a depth of only 10% from the total oxide thickness [21]. In the present study, where the total layer thickness is 15 nm maximum, it is likely that the amount of B^{3+} is sufficiently low for being outside the XPS detection limit. The anodic oxide grown in CB, with the XPS spectra presented in Fig. 3(b), shows a very similar behaviour to the one grown in BB. No clear indications of electrolyte incorporation could be concluded here as well. In contrast, when Ta was anodized in PB (part (c) of the figure) the presence of P could be clearly observed and it was quantified to approximately 5.5 at. %. The P 2s peak found at approximately 134 eV was reported in the literature to represent a P–O bond, confirming the incorporation of P into the oxide as a charged $(PO_4)^{3-}$ oxyanion [30], in agreement with reports based on electrochemical studies [21].

High-resolution spectra of Ta 4f doublet (presented in supplemental Fig. S2) suggest that all Ta oxides are stoichiometric. Moreover, no significant shifts were observed when comparing the doublet position from anodic oxides grown in different electrolytes with the position of Ta_2O_5 sputtered in identical conditions from a stoichiometric oxide target. No additional peaks at binding energies in the vicinity of the $4f_{7/2}$ peak (26.0 eV) are present, demonstrating the absence of Ta species in an oxidation state other than 5+ [31]. High-resolution spectra of O 1s

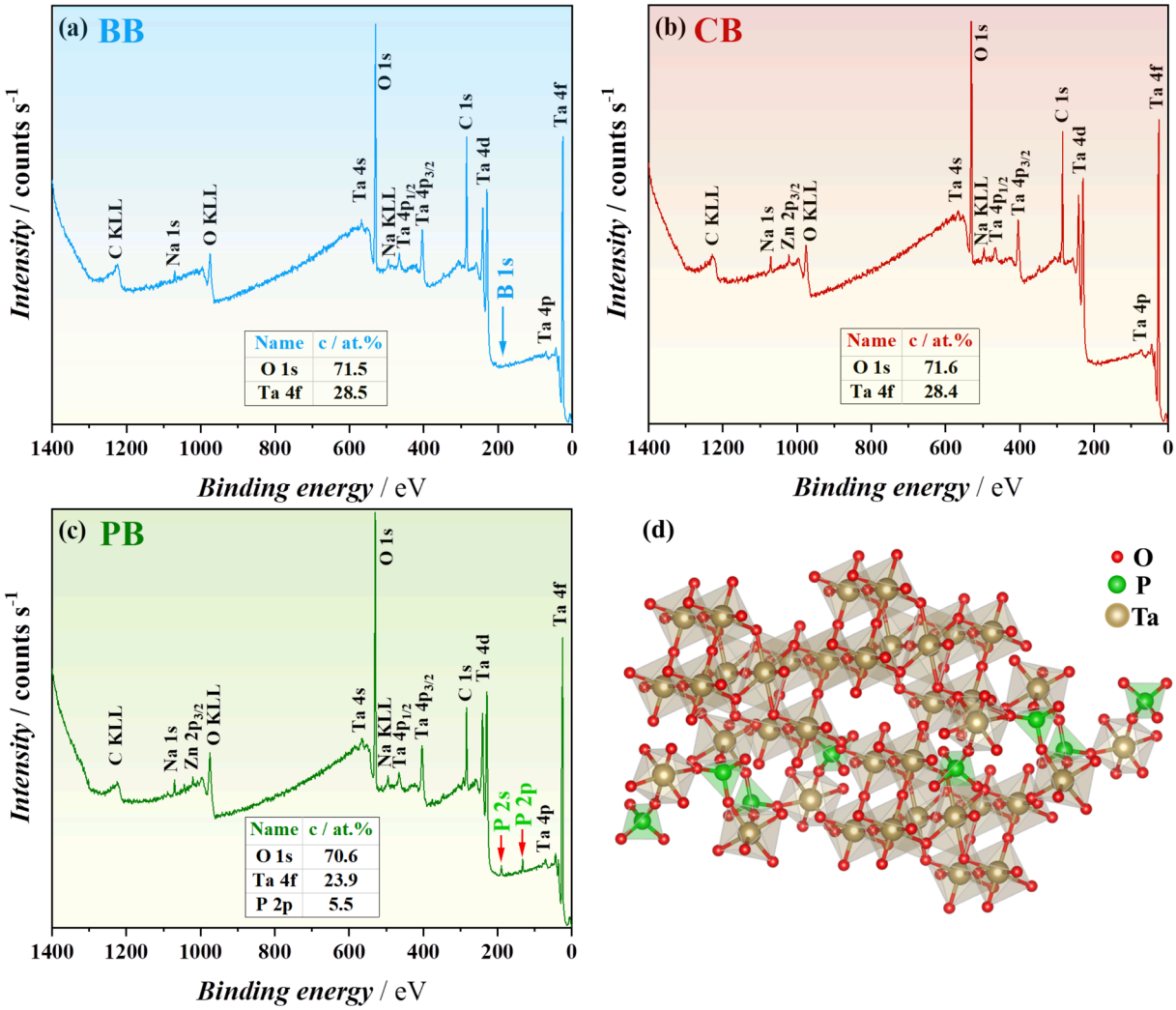

Fig. 3. XPS survey spectra and composition of Ta oxides grown in different electrolytes (a–c) and the model of the atomic structure of $TaOPO_4$ in Ta_2O_5 matrix (d).

peaks are presented in the supplemental Fig. S3. In all cases, a small shoulder normally attributed to O in bridge positions was observed, and this shoulder was shifted toward lower energies only in the case of oxides grown in PB [32]. Again, this indicates the presence of the Ta oxyphosphate as previously discussed. The quantifications for the samples grown in BB and CB lead to an approximate concentration of 29 at. % Ta and 71 at.% O which also points toward the formation of stoichiometric Ta_2O_5. This holds true also for the PB sample, for which no additional peak in the high-resolution spectrum of Ta 4f was found, indicating the formation of a phosphate-containing compound, which respects the 5+ valence of Ta. This compound forms simultaneous with Ta_2O_5 and it is most likely Ta oxyphosphate [31,33]. Visualization for Electronic and Structural Analysis software (VESTA) was employed to visualize and to observe the amount of incorporated $(PO_4)^{3-}$ based on the atomic concentrations obtained from XPS [34]. Since the oxides are amorphous [35], only short-order atomic arrangement was simulated. The $TaOPO_4$ embedded in a Ta_2O_5 matrix is shown in Fig. 3(d). The ratio of P to Ta atoms as obtained from XPS is approximately 6 to 24, which translates into one P atom per 4 atoms of Ta and further leading to roughly 2 $TaOPO_4$ for every 3 Ta_2O_5. The proposed proportion could be additionally testified by the O and Ta atoms ratio which is 25/8 and agrees well with the XPS data presented in Fig. 3(c). This indicates a relatively high amount of oxyphosphate incorporation into the anodically grown thin film, a fact which is expected to have an influence on the memristor properties. As it will be shown further by electrical testing the presence of electrolyte species inside the active layer in the case of PB increases the stability of the memristor. It could be assumed that phosphate assists the redox processes occurring during the hi-low states memristive transition. The O vacancies in this case have increased effective mobility since their number is higher due to the phosphate presence.

Description of the Ta anodic oxidation process in phosphate-containing electrolyte was recently updated by a quantitative point defect model (PDM) describing the formation of a bi-layered oxide (the thicknesses of the oxides were ranging from 7 nm to 30 nm). The suggested model is explaining point defect generation and annihilation reactions at the metal/oxide and oxide/electrolyte interfaces and supports the present expectation for improved memristive behaviour [36]. It was confirmed that the produced mobile O vacancies at the metal/oxide interface, which were also reported as responsible for enhancing the memristive effect, are controlling the formation of the inner layer grown into the metal. The outer layer is distinctly formed at the oxide/electrolyte interface by hydrolysed Ta interstitials and anions [36]. In the current work, the oxide layer was formed in aqueous solutions of Na_2HPO_4 and NaH_2PO_4 resulting in a mixture with acidic character. Therefore, it can be assumed that the growth mechanism of anodic oxide is equivalent to the reported findings considering that phosphate-containing electrolyte with acidic character was used. The acidic character is due to the HPO_4^{2-} ion defining a weak acid and the larger driving force of $H_2PO_4^-$ ion to dissociate rather than hydrolyse. Such an electrolyte environment could possibly assist the formation of Ta oxyphosphate, which is usually used as a solid acid catalyst obtained in the reaction with $C_4H_6O_6$ and Ta_2O_5 as a source of Ta [33,34,36]. In the case of 1 M PB solution, Randall et al. already concluded that the anodic film is a mixture of Ta_2O_5 and Ta oxyphosphate [33]. In the current work, the presence of Ta oxyphosphate additionally confirmed by XPS is assumed to lead to conservation of the original position of O atoms relative to the metal interface, as previously discussed by Pringle and Amsel, thus leading to CFs pinning [36–38]. Considering this argument, a pinned CF will not change its 3D location during its redox cycle (HRS-LRS switching). In this way, the position of CFs will be pre-defined by the anodic oxide growth leading to their improved stability by simply tuning the electrochemical parameters and electrolyte selection. Incorporation of species from the electrolyte (which are not complexing agents but solution-phase species originating from the phosphate) will improve the stability of the oxide layer, which in turn may impact the electrical stability and overall quality of PB memristors.

3.2. Effect of potentiodynamic anodization rate on memristive behaviour

In order to assess the electrolyte influence on the final memristive behaviour of Ta_2O_5, different electrolytes were used for potentiodynamic oxide formation at different rates of potential increase (scan rates). Examples of typical current-voltage (*I-U*) sweeps performed on anodic memristors (oxidized at up to 8 V *vs.* SHE) in PB, CB, and BB at various scan rates are presented in Fig. 4(a–c). The sweeps were recorded under limiting current conditions using different compliance values up to 5 mA. Generally, increasing the voltage range resulted in an irreversible dielectric breakdown of the Ta_2O_5. For this reason, in the entire study the voltage range never exceeded the ±2 V limit. The switching was accomplished in cycles as illustrated by the insets of Fig. 4 (a–c). The sweep direction is indicated by arrows, always starting from 0 V and moving in positive direction first until switching from HRS to LRS occurs. The LRS and HRS are observable in each case through the changing slope of the *I-U* curves. As previously mentioned, these define the SET (ON) and RESET (OFF) processes, respectively, when the charge transport through the memristor changes. The resulting hysteresis clearly defines a bipolar memristive switching, which is in agreement with previous reports [39]. At lower current compliances (see PB curve in Fig. 4(a)) the curves are asymmetric and the symmetry increases as soon as more current is allowed to pass through Ta_2O_5. Memristive behaviours were identified for all studied cases and the influence of different scan rates can be directly noted.

The HRS and LRS values directly measured from the *I-U* slopes for different scan rates are plotted in Fig. 4(d), while in Fig. 4(e) the HRS/LRS ratios are given for different anodization speeds. The differences between HRS and LRS for devices with oxides formed at 10 mV s^{-1} in different electrolytes (Fig. 4(a, d)) are small, except the PB case where the HRS/LRS ratio is almost 100 (Fig. 4(e)). Overall, BB electrolyte produced the most conductive memristors while anodization in PB resulted in the highest ohmic value for HRS. Increasing the scan rate to 100 mV s^{-1} resulted in Ta_2O_5 memristors with more consistent values of HRS close to 10 kΩ. Only BB electrolyte showed slightly more conducting HRS, just above 1 kΩ. When compared to the 10 mV s^{-1} case, the differences between HRS and LRS are much stronger for 100 mV s^{-1}. Increasing the scan rate to 1000 mV s^{-1} produced unstable memristive effects for all electrolytes. Even though memristive switching was possible (Fig. 4(c)), the reproducibility of CFs formation was very low. Generally, no reliable data was obtained from anodic memristors grown at the fastest scan rate of 1000 mV s^{-1}.

The values of LRS (except the PB 10 mV s^{-1} case) were constant regardless of the scan rate and electrolytes used for anodization but HRS values decreased for the highest scan rate. This may indicate that the overall electrical conductivity of devices increases for scan rates above 100 mV s^{-1} or that the charge carrier transport is enhanced for devices grown at 1000 mV s^{-1}. According to the switching mechanism of memristors, additional vacancies might be generated during the formation of the oxide layer at higher scan rates [40]. The middle and lower scan rate values were reported as forming more stable anodic oxides for valve metal [41]. In this case, the stability refers to uniform thickness and slower dissolution of the oxide layer at lower scan rates, a higher degree of order with denser structure and increased barrier height for ion migration. Previous studies showed that amorphous anodic films on Ta are formed at almost 100% current efficiency in all electrolytes and demonstrated extraordinary chemical stability [26,38]. Generally, the anodic oxide growth may be affected by defects or non-uniformities in the barrier layer due to the presence of stress-causing local crystalline regions, cracks, or corrosion. The composition and pH of the electrolyte, scan rate, or other electrochemical parameters will play a crucial role in these outcomes. As proven, the oxide layer formed herein was uniform in thickness without any failures, but its properties were influenced by electrolyte and scan rate, thus influencing the

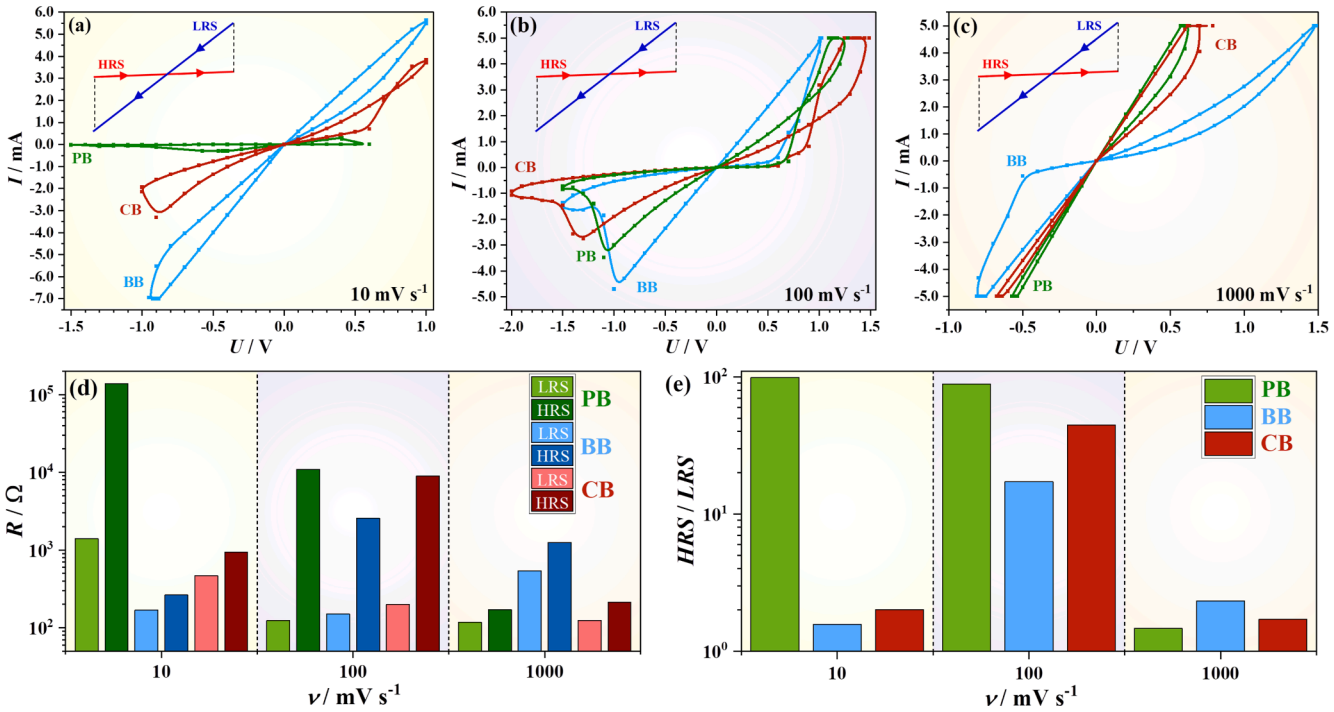

Fig. 4. Typical memristive switching curves for anodic memristors grown at 8 V in various electrolytes with different rates of potential increase (a–c). Values of HRS and LRS (d), and the HRS/LRS ratios (e).

memristive behaviour. It is suggested that at lower scan rates, more ordered oxides are grown benefiting the more stable CFs to form at constant positions However, too low rates may lead to enhanced chemical stability suppressing an efficient filament formation. In the current study, the most stable devices were formed at 100 mV s^{-1} favouring the highest difference between stable HRS and LRS [42,43] (Fig. 4(e)). For this reason, only this scan rate was taken as optimal and further used for an in-detail analysis of all electrolytes effect.

3.3. *Effect of final anodization potential on memristive behaviour*

According to the high field theory, the oxide growth factor for anodic Ta_2O_5 is a material constant, and in the current study it was measured as 1.8 nm V^{-1} in good agreement with previous electrochemical studies [35,45,46]. A relevant fact is that a constant behaviour during potentiodynamic oxide formation was previously reported, indicating a typical valve metal behaviour at potentials up to 8 V when barrier-type oxides are formed [47]. One of the goals of the present work is to compare memristive features of devices containing anodic films formed in various electrolytes applying different potentials, particularly 4 V (Ta_2O_5 thickness ≈ 8 nm) and 8 V (Ta_2O_5 thickness ≈ 15 nm). It is relevant to note that the formation factor of the oxide growth for valve metals at the potentials below 50 V is reported to change by less than 0.1 nm V^{-1} when using different electrolytes. For that reason, it is safe to assume that the resulting variation of the oxide layer thickness is below 5% [48,49].

An effect of oxide layer thickness on the achieved memristive performance is also expected. Short CFs may be easier to form, but multiple-level switching may require longer CFs. An optimal thickness value needs to be found for improving the memristive performance [50]. Fig. 5 (a)–(f) shows *I-U* sweeps of anodic memristive devices fabricated by anodization of Ta in various electrolytes. Each set of curves are plotted for different relevant current compliance values and the resulting memristive behaviours are directly observable in the figure. All three devices are showing bipolar switching and up to 4 distinguishable switching states were observed. However, the switching voltage range depends on the electrolyte used in the anodization process. The almost constant voltage values triggering the SET and RESET processes (for all analysed memristors) suggest good switching reproducibility for anodic Ta oxides, independent of electrolyte selection.

For all graphs collected in Fig. 5, the current is plotted in logarithmic scale for facilitating the observation of different memristive states, as given by various current levels for one fixed voltage. One can see a clear influence of the oxide layers thickness (8 and 15 nm for 4 and 8 V, respectively) for different electrolytes on memristive switching characteristics. Fig. 5(a, b) represent switching capabilities of anodic memristors formed in PB at potentials of 4 and 8 V. Memristive switching was successful for two different values of current compliances (Fig. 5(a)) when the thinnest oxide was used as active layer. The use of higher compliances resulted in an irreversible dielectric breakdown of the anodic memristors. Thicker oxide layers showed at least four different switching levels depending on the compliance (Fig. 5(b)). This is an important result linked to ReRAMs devices which may simulate an analog behaviour (storage of more than one bit per cell) allowing the variability of the programmed resistance states [51,52]. In contrast, a tendency of increasing multi-level switching states for thinner active layers is noticed for oxides grown in BB (Fig. 5(c)), while devices formed in CB showed two levels for both thinner and thicker oxide layers (Fig. 5 (e, f)). Hence, the thickness of the oxide layers combined with electrolyte selection has influenced the memory characteristics of memristors dramatically. Devices formed in different electrolytes require thickness optimization to examine the possibility of multi-level switching. Nevertheless, the most superior performance was confirmed for memristors anodized in PB at 8 V, suggesting that incorporation of phosphorous confirmed by XPS measurements (Fig. 3(c)) may benefit electrical and memory characteristics of Ta devices.

A comparison between HRS and LRS can be easily done using data presented in Fig. 5 for different memristors and the highest HRS/LRS ratio (up to 3 orders of current *I* magnitude) is hinted for oxides grown in PB electrolyte. The second largest ratio can be attributed to the use of BB electrolyte, where still one order of magnitude can be seen. The use of CB electrolyte proved to be the least favourable in terms of the HRS/LRS ratio where the values dropped below 10. Such findings are somehow surprising given that most of the previous literature reports

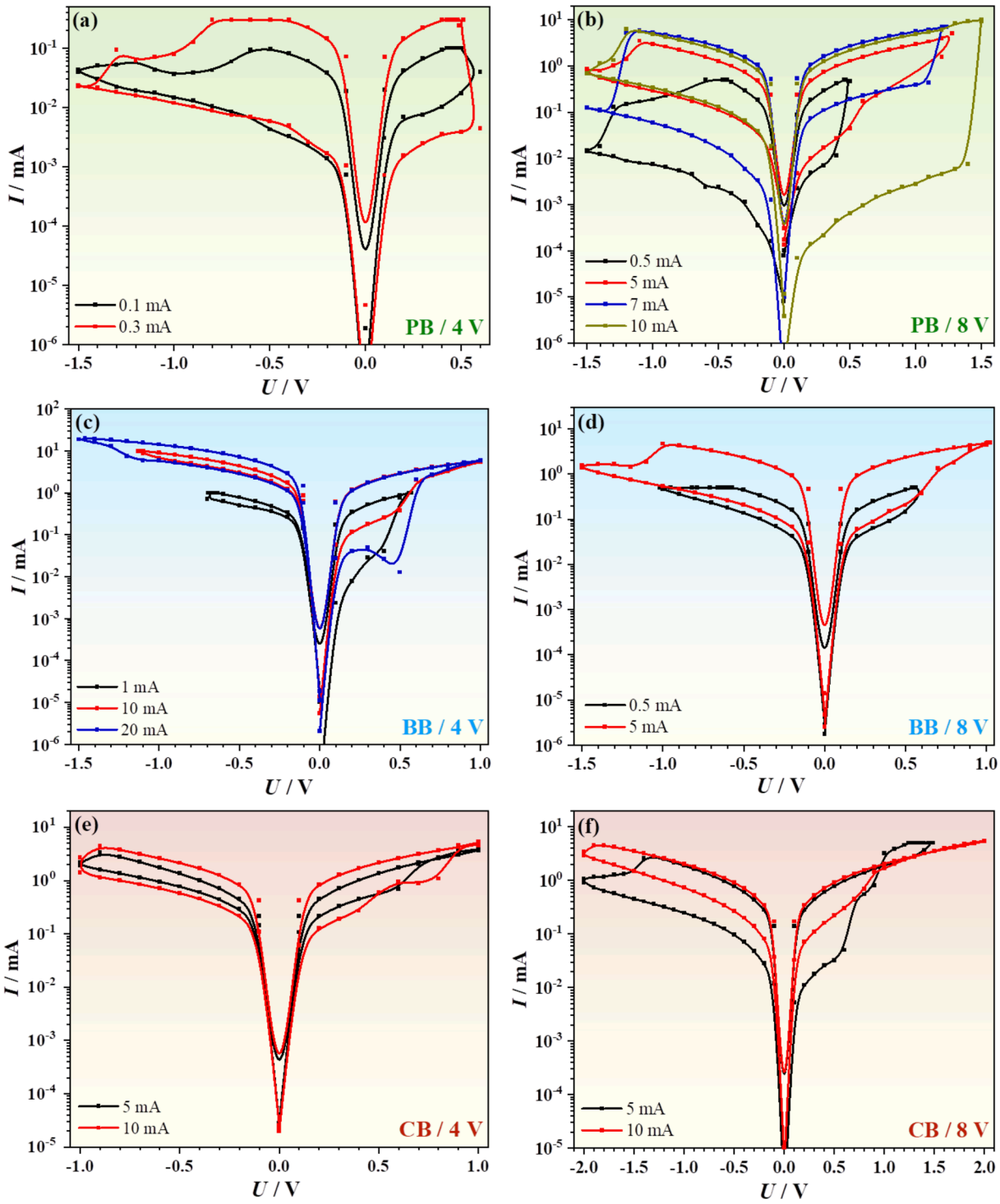

Fig. 5. *I-U* sweeps of anodic memristors grown in different electrolytes (100 mV s^{-1}) at different anodization potentials (anodic oxides with different thicknesses).

communicate a ratio slightly above 10 for Ta oxides grown in BB or PB electrolyte [19,20]. This is clearly pointing out the crucial role the electrolyte plays in the electrical behaviour of the anodic memristor. Changing anodization parameters directly affects the dynamic of oxide growth impacting its performance in solid-state devices [53].

3.4. Electrolyte incorporation influence on device lifetime

One of the most relevant characteristics of a memristor is its endurance, defined by the maximum number of HRS to LRS switching cycles before irreversible dielectric breakdown occurs. Endurance testing for all anodic memristors under study was performed by direct measuring HRS and LRS values as a function of switching cycles. Additionally, if full switching can be regarded as a "write" procedure (a term borrowed from ReRAMs) a "read" procedure will be described by a pure electrical assessment (usually at low voltages) of the present state/resistance value. In other words, after SET or RESET the memristor resistance is measured (without state switching) many times in a row and the result is presented also as HRS or LRS value depending on read cycles. This characterizes the retention of the anodic memristor and is an

important parameter to consider for the quality assessment of a device. The fact that the read cycle does not change the information contained in one storage cell is an important advantage of memristive devices when compared to magnetic hard disks or transistor-based storage cells which need to be rewritten after each single read cycle.

Endurance and retention performance of anodic Ta_2O_5 memristive devices oxidized at 8 V (100 mV s^{-1} scan rate) are presented in Fig. 6. The electrolyte and the write/read procedure are specified for each graph. Endurance up to 10^6 cycles without degradation of LRS and HRS was clearly identified for memristors formed in PB. As described before, more than two orders of magnitude can be easily calculated for the HRS/LRS ratio, the memristor changing its resistive state from below 100 Ω to more than 10 kΩ. The memristor with the oxide grown in BB showed stronger instabilities for both HRS and LRS values. The HRS/LRS ratio is smaller, but resistance values for both states are distinguishable. The HRS becomes more conductive with increasing switching cycles approaching LRS values above 10^5 cycles and defining a rather limited lifetime in these conditions. Endurance testing of oxides grown in CB allowed switching up to 10^4 cycles. However, in this case, the HRS/LRS ratio was much larger as compared to the BB case and the switching

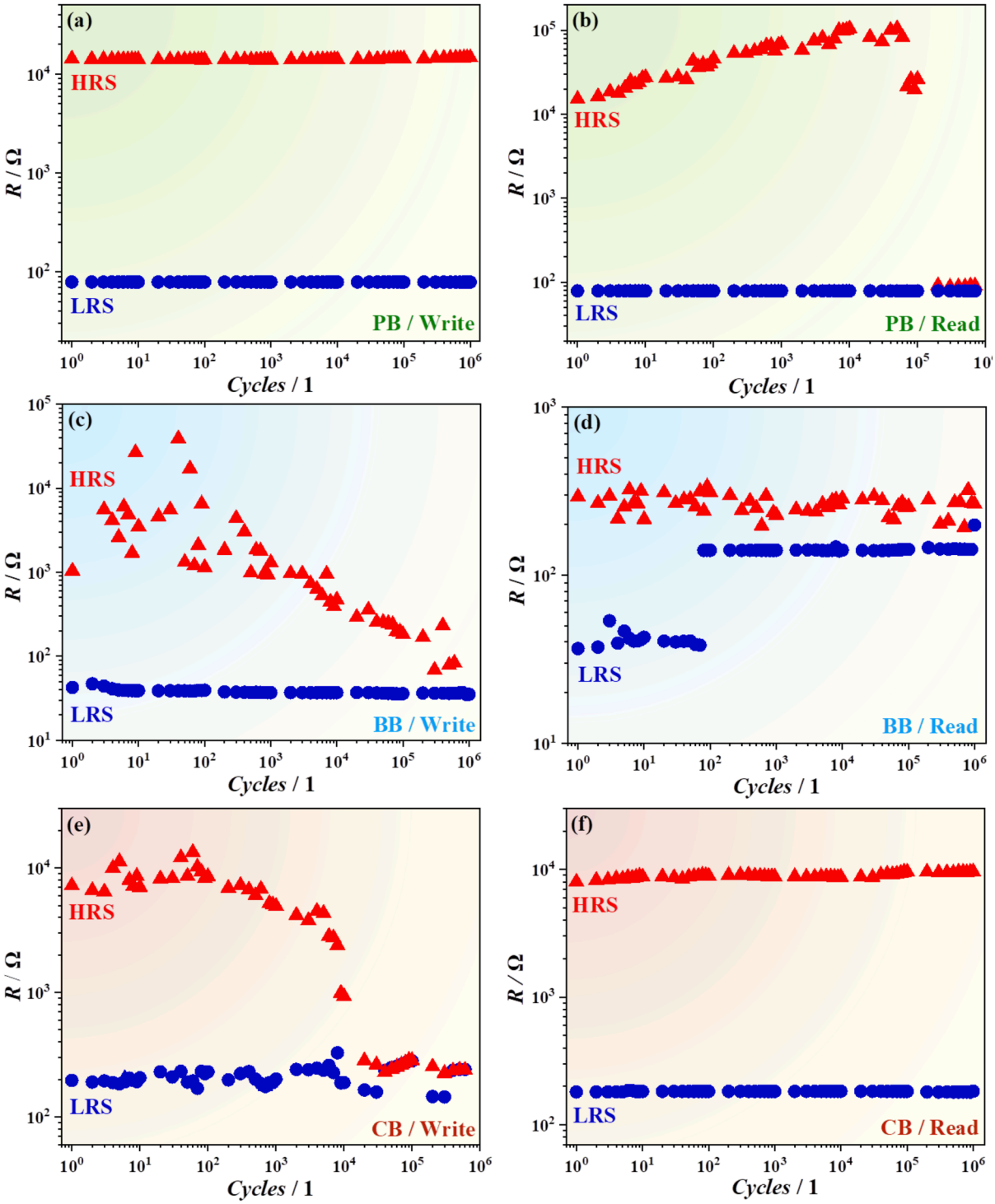

Fig. 6. Endurance (writing) and retention (reading) testing on anodic memristors grown in different electrolytes (100 mV s^{-1} at 8 V).

occurred in ohmic ranges similar to the memristors grown in PB electrolyte. After 10^4 cycles the HRS degrades becoming indistinguishable from the LRS, most likely indicating irreversible dielectric breakdown.

Retention tests were performed on separate devices grown in the same conditions as those assessed for their endurance. A direct comparison and/or correlation can be done in Fig. 6 where the "read" procedure is indicated together with the electrolyte. In all cases, the retention test of HRS was performed immediately after the retention test of LRS on the same device and the resistance was always read by applying a very low voltage. Excepting the BB memristor, at least up to 10^5 read cycles confirmed the retention of HRS without degradation. A significant decrease in resistance stability appeared after 10^5 cycles for the PB anodized Ta, when the device could not discriminate the states anymore. The case of using BB electrolyte resulted in instabilities, similar to those observed during the write procedure. Despite the sudden increase of the LRS values which were observed only after 10^2 cycles, the maximum number of read cycles was in the range of 10^6. These variations were reported to be triggered by thermodynamic instabilities of CFs manifested as a sudden increase of LRS during the retention time [50]. The sample anodized in CB exhibited the highest reading stability for both LRS and HRS (more than 10^6 cycles). As previously reported, the anodic oxides grown in CB demonstrate excellent stability and uniformity showing n-type semiconducting behaviour [26]. It may even be argued that this is beneficial for the stability of HRS and LRS of the devices which are not suffering from thermal disturbance of CFs as in the case of devices formed in BB. However, the current findings suggest that such oxides may not provide enough mobile species to be transported through the conductive pathway, as given by the HRS/LRS ratio when compared to the oxides formed in PB and BB. In fact, the overall conductance of the device was not increased suggesting that the oxygen vacancies concentration was constant. Otherwise, the retention failure would have happened sooner [50]. Following this reasoning and according to the literature, the mobility values of electrolyte species incorporated in the anodic oxides may be appreciated as the highest for PB, smaller for BB, whereas inconclusive for CB electrolyte [21]. As it was previously discussed in the current work, only P incorporation was confirmed by XPS (Fig. 3(c)). Furthermore, it was also concluded that the oxides formed at optimally low scan rates, depending on the electrolyte composition, may have more ordered structures. Accordingly, devices with the oxides formed in PB and CB at 100 mVs^{-1} showed the highest HRS/LRS ratio (see Fig. 4e). Due to the Ta oxyphosphate formation in oxides grown in PB, the anodic oxide atomic arrangement may be affected, thus benefiting CFs positioning and writing stability. Additionally, this may be supported by higher mobility of O vacancies moving through CFs. However, such a structure of the oxide layer is more complex. Once the devices are left in HRS or LRS for a number of reading cycles, the reading stability may be limited due to the sudden diffusion of O vacancies nearby the Ta oxyphosphate formation regions [50]. Since no electrolyte species incorporation was confirmed in anodic oxide layers grown in CB, it may be assumed that such events were avoided resulting in better retention performance. This can be better illustrated with the switching mechanism based on the consecutive oxidation - reduction reactions at the metal/electrolyte interface, responsible for CFs formation (see Section 3.6). The higher the amount of mobile O vacancies, the easier is their movement through CFs and consequently easier switching from HRS to LRS and vice versa. In this regard, it is expected that device lifetime ends up sooner if an unlimited amount of O vacancies is outsourced into CF at random positions in the oxide leading to its irreversible rupture. Additionally, O vacancies may interfere with the species of complex structure in defined CFs regions by Ta oxyphophate, which makes the reading of a current resistance state more difficult. In other words, the presence of CFs pinning decreases the probability of irreversible CFs rupture. Even though CB appears to be the best electrolyte choice for high retention times, the lower endurance (due to CFs formation at random locations between consecutive switching cycles) would limit the device lifetime. As the best compromise, PB electrolyte should still be preferred for devices due to its longest endurance in spite of shorter retention.

3.5. Conductive filaments imaging

For deeper insights into the memristor structure peculiarities, rigorous TEM investigation has been fulfilled. Since only anodic memristors grown in PB have incorporated electrolyte species, their imaging was performed. Before imaging, the PB memristor was switched to the HRS. In Fig. 7 TEM imaging of the sample preliminary characterized chemically in Fig. 2 is presented. An overview of the layers morphology in cross-section geometry is provided in part (a) of the figure complementing the SEM (Fig. S1) and TEM images briefly discussed previously in Fig. 1(c). One can see that initially, Ta film had a rather wavy surface (in the nm range) that could be considered from the shape of the interface between the anodic oxide layer and the Pt one grown after oxidation. Such morphology is predicted and expected considering the columnar structure of Ta film (visible in Fig. 7(a)) usually obtained by sputtering. In detail imaging of the Ta_2O_5 layer reveals some special areas such as one marked with a red square and presented in Fig. 7(b).

The HRTEM image shows that both metallic electrodes (Pt on top and Ta below) have polycrystalline characteristics with distinguishable grains while the anodic oxide is amorphous. Tilting the sample allows highlighting the crystalline droplet-shaped region with the location of three filaments radially connected to it (area designated with a blue square in Fig. 7(b)). Such filaments are much easier observable in polycrystalline oxides, such as TiO_2 as was previously reported [54]. In the case of Ta_2O_5, the amorphous character of the filaments due to switching to HRS and the surrounding amorphous anodic oxide makes visualization of their location challenging, but not impossible. In order to address this challenge and ease CFs observation, an FFT analysis of the region of interest has been performed and the results are presented in Fig. 7(c). Thus, one can see the general FFT pattern of the blue square region. Then the special mask has been applied. The main idea behind this mask was first - to highlight crystalline structure by selecting the distinct reflexes and second - to minimize the so-called salt-pepper contrast specific to an amorphous phase. The IFFT image constructed using the mentioned mask is provided in the inset. For better visualization, the pairs of red lines, connecting the Pt protrusion with the bottom Ta layer, highlight the regions in which CFs are localized. Regardless of the amorphous Ta oxide, the charge passing through filaments during the HRS/LRS transition has an influence on the local atomic order around the conductive paths, and close observation of the TEM images enhanced by the applied FFT analysis could reveal them.

The next step of analysis that must be performed is the unraveling of the crystalline droplet-shaped region structure. This analysis is particularly important since recent findings in anodic Hf memristors describe such interfacial zones as accumulation regions from which CFs grow [55]. The resolution of EDX mapping applied in the frame of the study was not enough to distinguish the material located there in a faithful manner. In this regard, FFT analysis can provide more reliable data. Indexed FFT pattern together with IFFT in the inset (green frames) reveals a crystal structure correspondent to Pt [56]. This observation could bring more light to the specification of favourable sites for CFs formation. Many grain boundaries in the polycrystalline Ta bottom layer are visible in Fig. 7(a). However, considering that only a few prominent CFs regions were found, it can be assumed that the preferred positions for CFs formation are determined by the conjunction of multiple factors and are not governed solely by the grain-boundary locations. Consequently, gathering more statistics on the observed phenomenon is crucial for deeper insight and would be addressed in the frame of future studies.

In general, the memristors containing Ta_2O_5 as an insulating layer behave as valence change memories (VCM) [57]. The conductive filaments formation and rupture are described as a consequence of oxidation - reduction reactions at the metal/electrolyte interface, thus generating O species migration. In this way, an O deficient CF is formed

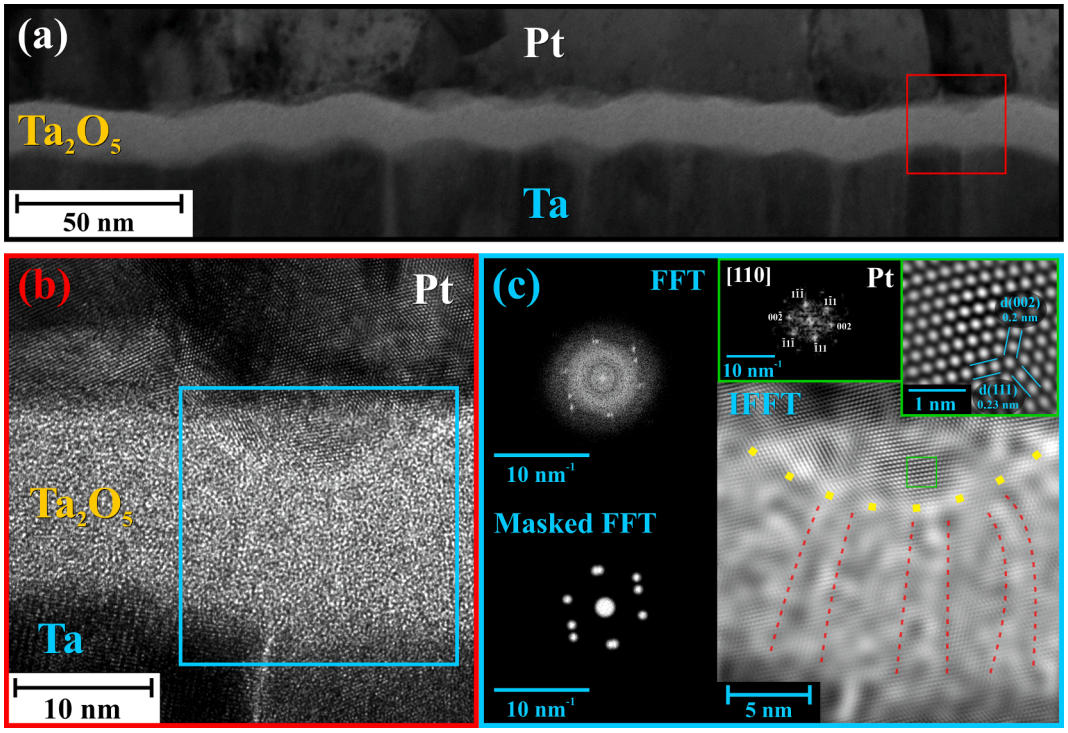

Fig. 7. TEM image of anodic memristor in HRS grown at 8 V, 100 mV s^{-1} in PB electrolyte. Overview BF image of a layered MIM structure (a) and HRTEM image of the amorphous oxide layer sandwiched between polycrystalline Pt and Ta (b). FFT analysis of the region designated with blue square revealing a Pt protrusion (yellow dashed line) and several conductive filaments (localized in the regions between red dashed lines) (c). (For interpretation of the references to colour in this figure legend, the reader is referred to the web version of this article.)

and present during the resistive switching to LRS, whereas its re-oxidation/dissolution causes the event of switching to HRS. This process is schematically described in Fig. 8. However, the movement of cations may support the switching mechanism as well [7,20]. In the current work, the formation of Ta oxyphosphate may benefit the CFs pinning and explain the higher endurance of anodic memristors formed in PB.

As it was mentioned previously, the average Ta_2O_5 layer thickness grown in PB at 8 V is ≈15 nm, while in the vicinity of these Pt protrusions the oxide layer seems to be thinner (≈11 nm). That may affect the concurrency of CFs formed at constant positions. However, this thickness is still bigger than the one in the 4 V anodization potential case (8 nm), thus it could be assumed to provide 'enough space' for CFs concurrency. Such concurrency was recently identified in anodic memristors grown on Hf as well [55], and is probably responsible for the observed multi-level switching in Fig. 5b. At the same time, to avoid ambiguity, further comprehensive investigation of the CFs formation sequences together with the effect of oxide layer thickness on the achieved memristor properties is still vital. According to the results showing high performance of memristors fabricated in PB, the formation of concurrent CFs at the constant positions may prevent device failure due to the sudden diffusion of oxygen vacancies during switching between HRS and LRS in cycles [49] as already explained in Section 3.1.

3.6. Electrolyte selection

In order to decide which conditions are the best for memristor fabrication, both electrical and memory characteristics should be considered. The relevant characteristics are summarized in Fig. 4(e) and Fig. 5 where the HRS/LRS ratio and the number of distinguishable

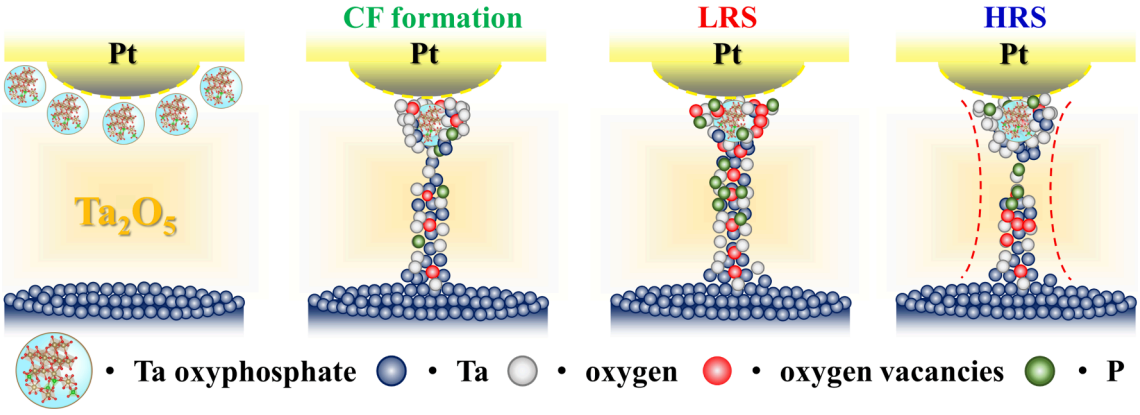

Fig. 8. Schematic of the memristive switching mechanism in anodic Ta oxide memristors grown in PB electrolyte. The guiding red dotted lines highlight CFs localization (similar to Fig. 7). (For interpretation of the references to colour in this figure legend, the reader is referred to the web version of this article.)

switching levels are seen for each electrolyte and each anodization condition. Regardless of the rate of potential increase, the HRS/LRS ratio always depended on the chosen electrolyte decreasing in the order: PB, BB, and CB. The absolute values, however, are conditional on the anodization rate and the highest ratios are observed for 100 mV s^{-1} when the use of PB electrolyte led to the HRS/LRS ratio of more than 100. The slowest and fastest anodization rates generally produced similar results, except the PB case when only fast anodization resulted in very small ratios, which are adverse for memristor performance. One can remind once again that the utilization of PB produced four levels while BB produced up to three and CB produced maximum two distinguishable switching levels. The number of switching levels can be evaluated from Fig. 5.

In order to better follow these arguments, Fig. 8 summarizes different relevant aspects of memristors formed in PB. For closer observation of the HRS/LRS cycling process, exemplifying switching curves recorded during endurance testing are presented in Fig. 9(a). For a current compliance of 10 mA, up to 10^4 switching cycles did not substantially affect the HRS/LRS ratio. However, this ratio is slightly smaller for the first cycle, when the LRS is not sufficiently conductive, and for the last cycle, when the HRS is not sufficiently insulating. Fig. 9(b) represents classical *I-U* sweeps immediately after formation (the cycling direction is shown in the inset) confirming four distinguishable switching levels. Different slopes can easily be observed when comparing the curves. However, variations of the four switching levels were observed between different devices. Fig. 9(c) is a representation of LRS values for these levels extracted from endurance measurements of randomly chosen devices up to 10^6 cycles. The error bars are empirically determined by observing inter-device variations. If the lowest and highest resistive levels are well reproducible from one memristor to the next, the intermediate ones have overlapping confidence bands, in spite of their reproducible switching for one given device. This emphasizes the importance of initial memristor formation that includes certain material fatigue, usually obtained after a few full switching cycles.

The end lifetime for a memristor is defined by the presence of a more conductive HRS due to formation of irreversible CFs resulting from material fatigue. Following this reasoning and the findings of the current research it can be concluded that the most promising multi-level anodic memristor with the highest HRS/LRS ratio, should be grown in PB electrolyte at 100 mV s^{-1}. This is supporting the statement about the beneficial effect of Ta oxyphosphate formation allowing CFs pining at the constant positions inside the anodic oxide layer. This finding may play a crucial role in the possibility to predict CFs positioning during the memristor formation step. Therefore, further studies of Ta anodic oxide formed in PB such as pH and concentration optimization and imaging of CFs may improve anodic Ta memristors in the way that their operation may reach the level of Ta memristors fabricated via more demanding methods (e.g. sputtering or ALD).

4. Conclusions

The current study compares the electrolyte influence on the memristive behaviour of anodic Ta oxide grown in different conditions directly on Ta serving as the bottom electrode. Patterning Pt top electrodes after anodization of Ta thin films finalizes a straightforward device fabrication procedure. The findings presented and discussed allow assuming that the electrochemical parameters during potentiodynamical anodization directly influence the electrolyte species incorporation inside the anodic oxide, and thus permit tuning the device properties. A great improvement in the performance and memory characteristics of Ta anodic memristors is attributed to the phosphate electrolyte used for their fabrication at 100 mV s^{-1}. Conductive filaments in HRS and the structure of the oxide layer were successfully observed by high-resolution TEM and highlighted applying FFT analysis. The enhancement of memristive behaviour of oxides anodized in PB could be consistently justified by a higher number of O vacancies due to the formation of Ta oxyphosphate. The suggested bipolar switching mechanism was supported by the oxyphosphate formation which is strongly believed to cause spatial pinning of conductive filaments positions during the redox read/write process. Hence, it can be concluded that the properties of Ta anodic memristors fabricated in a simple and cost-effective manner, can be considered as strong candidates for further ReRAMs applications.

Impact statement

Understanding the role of electrolyte incorporation (borate, citrate, or phosphate) in anodic Ta_2O_5 memristors allows a proper selection for applications. Phosphates incorporation enhances memristive characteristics due to the presence of Ta oxyphosphate, while no additional fabrication requirements are necessary.

CRediT authorship contribution statement

Ivana Zrinski: Conceptualization, Data curation, Formal analysis, Investigation, Validation, Writing - original draft, Writing – review & editing. **Alexey Minenkov:** Conceptualization, Investigation, Visualization, Methodology, Validation, Writing – original draft, Writing – review & editing. **Cezarina Cela Mardare:** Methodology, Investigation, Validation, Writing – original draft, Writing – review & editing. **Jan Philipp Kollender:** Methodology, Validation, Writing – original draft. **Shaukat Ali Lone:** Investigation, Writing – original draft. **Achim Walter Hassel:** Methodology, Resources, Validation, Writing – review & editing. **Andrei Ionut Mardare:** Conceptualization, Data curation, Formal analysis, Funding acquisition, Investigation, Methodology, Project administration, Resources, Software, Supervision, Validation, Writing – original draft, Writing – review & editing.

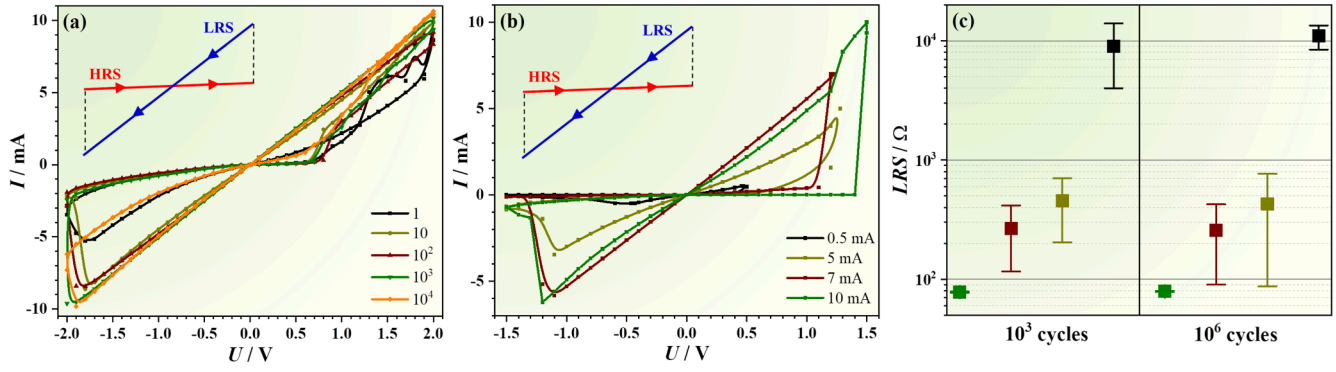

Fig. 9. Example of *I-U* sweeps of anodic memristors recorded during endurance measurements (a), multi-level switching obtained by recording *I-U* sweeps at different current compliances for anodic memristors formed in PB (b) and their LRS values extracted from endurance measurements presenting different resistive switching levels (c).

Declaration of Competing Interest

The authors declare that they have no known competing financial interests or personal relationships that could have appeared to influence the work reported in this paper.

Acknowledgements

This research was funded in whole, or in part, by the Austrian Science Fund (FWF) [P32847-N]. For the purpose of open access, the authors have applied a CC BY public copyright license to the Accepted Manuscript version arising from this submission. The experimental support (FIB and TEM) of Günter Hesser and Peter Oberhumer from the Zentrum für Oberflächen- und Nanoanalytik (ZONA) at Johannes Kepler University Linz are gratefully acknowledged.

Appendix A. Supplementary material

Supplementary data to this article can be found online at https://doi.org/10.1016/j.apsusc.2021.150608.

References

[1] M.M. Rehman, H.M.M.U. Rehman, J.Z. Gul, W.Y. Kim, K.S. Karimov, N. Ahmed, Decade of 2D-materials-based RRAM devices: a review, Sci. Technol. Adv. Mater. 21 (2020) 147–186, https://doi.org/10.1080/14686996.2020.1730236.
[2] J.J. Yang, D.B. Strukov, D.R. Stewart, Memristive devices for computing, Nat. Nanotechnol. 8 (2013) 13–24, https://doi.org/10.1038/nnano.2012.240.
[3] X. Sheng, C.E. Graves, S. Kumar, X. Li, B. Buchanan, L. Zheng, S. Lam, C. Li, J. P. Strachan, Low-conductance and multilevel CMOS-integrated nanoscale oxide memristors, Adv. Electron. Mater. 5 (2019) 1–8, https://doi.org/10.1002/aelm.201800876.
[4] Y. Wang, G. Ding, J.Y. Mao, Y. Zhou, S.T. Han, Recent advances in synthesis and application of perovskite quantum dot based composites for photonics, electronics and sensors, Sci. Technol. Adv. Mater. 21 (2020) 278–302, https://doi.org/10.1080/14686996.2020.1752115.
[5] N.K. Upadhyay, H. Jiang, Z. Wang, S. Asapu, Q. Xia, J. Joshua Yang, Emerging memory devices for neuromorphic computing, Adv. Mater. Technol. 4 (2019), https://doi.org/10.1002/admt.201800589.
[6] T. Hino, T. Hasegawa, K. Terabe, T. Tsuruoka, A. Nayak, T. Ohno, M. Aono, Atomic switches: atomic-movement-controlled nanodevices for new types of computing, Sci. Technol. Adv. Mater. 12 (2011), https://doi.org/10.1088/1468-6996/12/1/013003.
[7] R. Waser, M. Aono, Nanoionics-based resistive switching memories, Nanosci. Technol. A Collect. Rev. Nat. J. (2009) 158–165, https://doi.org/10.1142/9789814287005_0016.
[8] Y. Tao, Z. Wang, H. Xu, W. Ding, X. Zhao, Y. Lin, Y. Liu, Moisture-powered memristor with interfacial oxygen migration for power-free reading of multiple memory states, Nano Energy 71 (2020), 104628, https://doi.org/10.1016/j.nanoen.2020.104628.
[9] M. Lübben, P. Karakolis, V. Ioannou-Sougleridis, P. Normand, P. Dimitrakis, I. Valov, Graphene-modified interface controls transition from VCM to ECM switching modes in Ta/TaOx based memristive devices, Adv. Mater. 27 (2015) 6202–6207, https://doi.org/10.1002/adma.201502574.
[10] M. Lee, C.B. Lee, D. Lee, S.R. Lee, M. Chang, J.H. Hur, Y. Kim, C. Kim, D.H. Seo, S. Seo, U. Chung, I. Yoo, K. Kim, A fast, high-endurance and scalable non-volatile memory device made from asymmetric Ta2O5-x/TaO2-x bilayer structures, Nat. Mater. 10 (2011) 625–630, https://doi.org/10.1038/nmat3070.
[11] F. Miao, W. Yi, I. Goldfarb, J.J. Yang, M.X. Zhang, M.D. Pickett, J.P. Strachan, G. Medeiros-Ribeiro, R.S. Williams, Continuous electrical tuning of the chemical composition of TaO x-based memristors, ACS Nano 6 (2012) 2312–2318, https://doi.org/10.1021/nn2044577.
[12] J.A. Koza, Z. He, A.S. Miller, J.A. Switzer, Resistance switching in electrodeposited VO2 thin films, Chem. Mater. 23 (2011) 4105–4108, https://doi.org/10.1021/cm2019394.
[13] I. Zrinski, C.C. Mardare, L.-I. Jinga, J.P. Kollender, G. Socol, A.W. Hassel, A. I. Mardare, Phosphate incorporation in anodic hafnium oxide memristors, Appl. Surf. Sci. 548 (2021), https://doi.org/10.1016/j.apsusc.2021.149093.
[14] L. Mayr, N. Köpfle, A. Auer, B. Klötzer, S. Penner, An (ultra) high-vacuum compatible sputter source for oxide thin film growth, Rev. Sci. Instrum. 84 (2013), https://doi.org/10.1063/1.4821148.
[15] X.Y. Li, X.L. Shao, Y.C. Wang, H. Jiang, C.S. Hwang, J.S. Zhao, Thin TiOx layer as a voltage divider layer located at the quasi-Ohmic junction in the Pt/Ta2O5/Ta resistance switching memory, Nanoscale 9 (2017) 2358–2368, https://doi.org/10.1039/c6nr08470b.
[16] J.J. Yang, N.P. Kobayashi, J.P. Strachan, M.X. Zhang, D.A.A. Ohlberg, M.D. Pickett, Z. Li, G. Medeiros-Ribeiro, R.S. Williams, Dopant control by atomic layer deposition in oxide films for memristive switches, Chem. Mater. 23 (2011) 123–125, https://doi.org/10.1021/cm1020959.
[17] A. Niskanen, U. Kreissig, M. Leskelä, M. Ritala, Radical enhanced atomic layer deposition of tantalum oxide, Chem. Mater. 19 (2007) 2316–2320, https://doi.org/10.1021/cm0626482.
[18] S. Chen, S. Noori, M.A. Villena, Y. Shi, T. Han, Y. Zuo, M.P. Pedeferri, D. Strukov, M. Lanza, M.V. Diamanti, Memristive electronic synapses made by anodic oxidation, Chem. Mater. 31 (2019) 8394–8401, https://doi.org/10.1021/acs.chemmater.9b02245.
[19] A. Zaffora, F. Di Quarto, H. Habazaki, I. Valov, M. Santamaria, Electrochemically prepared oxides for resistive switching memories, Faraday Discuss. 213 (2019) 165–181, https://doi.org/10.1039/c8fd00112j.
[20] A. Zaffora, D.Y. Cho, K.S. Lee, F. Di Quarto, R. Waser, M. Santamaria, I. Valov, Electrochemical tantalum oxide for resistive switching memories, Adv. Mater. 29 (2017) 1–6, https://doi.org/10.1002/adma.201703357.
[21] K. Shimizu, K. Kobayashi, G.E. Thompson, P. Skeldon, G.C. Wood, Anodic oxide films on tantalum: incorporation and mobilities of electrolyte-derived species, Philos. Mag. B Phys. Condens. Matter; Stat. Mech. Electron. Opt. Magn. Prop. 73 (1996) 461–485, https://doi.org/10.1080/13642819608239129.
[22] M.V. Diamanti, M. Ormellese, M.P. Pedeferri, Application-wise nanostructuring of anodic films on titanium: a review, J. Exp. Nanosci. 10 (2015) 1285–1308, https://doi.org/10.1080/17458080.2014.999261.
[23] J.F. Vanhumbeeck, J. Proost, Current understanding of ti anodisation: functional, morphological, chemical and mechanical aspects, Corros. Rev. 27 (2009) 117–204, https://doi.org/10.1515/CORRREV.2009.27.3.117.
[24] W. Xue, Y. Li, G. Liu, Z. Wang, W. Xiao, K. Jiang, Z. Zhong, S. Gao, J. Ding, X. Miao, X.H. Xu, R.W. Li, Controllable and stable quantized conductance states in a Pt/HfOx/ITO memristor, Adv. Electron. Mater. 6 (2020) 1–9, https://doi.org/10.1002/aelm.201901055.
[25] S. Dirkmann, J. Kaiser, C. Wenger, T. Mussenbrock, Filament growth and resistive switching in hafnium oxide memristive devices, ACS Appl. Mater. Interfaces 10 (2018) 14857–14868, https://doi.org/10.1021/acsami.7b19836.
[26] Y.-H. Kim, K. Uosaki, Preparation of tantalum anodic oxide film in citric acid solution – evidence and effects of citrate anion incorporation, J. Electrochem. Sci. Technol. 4 (2013) 163–170, https://doi.org/10.5229/jecst.2013.4.4.163.
[27] Y.M. Li, L. Young, Effect of incorporated electrolyte species on the ac response of the high field ionic conduction process in anodic oxide films on tantalum, Electrochim. Acta 44 (1998) 605–611, https://doi.org/10.1016/S0013-4686(98)00183-2.
[28] Sodium phosphate, Cold Spring Harb. Protoc. 2006 (2006) pdb.rec8303. https://doi.org/10.1101/pdb.rec8303.
[29] K. Stella, S. Franzka, D. Bürstel, D. Diesing, D. Mayer, V. Roddatis, Electrochemical oxidation as vertical structuring tool for ultrathin (d < 10 nm) valve metal films, ECS J. Solid State Sci. Technol. 3 (2014) P143–P148, https://doi.org/10.1149/2.013405jss.
[30] R.S. Namur, K.M. Reyes, C.E.B. Marino, Growth and electrochemical stability of compact tantalum oxides obtained in different electrolytes for biomedical applications, Mater. Res. 18 (2015) 91–97, https://doi.org/10.1590/1516-1439.348714.
[31] Y.R. Denny, T. Firmansyah, S.K. Oh, H.J. Kang, D.S. Yang, S. Heo, J.G. Chung, J. C. Lee, Effect of oxygen deficiency on electronic properties and local structure of amorphous tantalum oxide thin films, Mater. Res. Bull. 82 (2016) 1–6, https://doi.org/10.1016/j.materresbull.2016.03.004.
[32] J. Wang, D. Ren, Z. Zhang, H. Xiang, J. Zhao, Z. Zhou, X. Li, H. Wang, L. Zhang, M. Zhao, Y. Fang, C. Lu, C. Zhao, C.Z. Zhao, X. Yan, A radiation-hardening Ta/Ta2O5-x/Al2O3/InGaZnO4 memristor for harsh electronics, Appl. Phys. Lett. 113 (2018) 2–6, https://doi.org/10.1063/1.5045649.
[33] J.J. Randall, The effect of phosphorus incorporation on the dielectric constant and ionic conductivity of anodic tantalum oxide, Electrochim. Acta 20 (1975) 663–667, https://doi.org/10.1016/0013-4686(75)90064-X.
[34] K. Momma, F. Izumi, VESTA 3 for three-dimensional visualization of crystal, volumetric and morphology data, J. Appl. Crystallogr. 44 (2011) 1272–1276, https://doi.org/10.1107/S0021889811038970.
[35] M.M. Lohrengel, **Thin anodic oxide layers on aluminium and other valve metals: high field regime**, Mater.Sci.Eng.R Rep. 12 (1993) 243–294, https://doi.org/10.1016/0927-796X(94)90011-6.
[36] J.D. Sloppy, Z. Lu, E.C. Dickey, D.D. MacDonald, Growth mechanism of anodic tantalum pentoxide formed in phosphoric acid, Electrochim. Acta 87 (2013) 82–91, https://doi.org/10.1016/j.electacta.2012.08.014.
[37] J.P.S. Pringle, The migration of oxygen during the anodic oxidation of tantalum, J. Electrochem. Soc. 120 (1973) 1391, https://doi.org/10.1149/1.2403268.
[38] G. Amsel, C. Cherki, G. Feuillade, J.P. Nadai, The influence of the electrolyte on the composition of “anodic oxide films” on tantalum, J. Phys. Chem. Solids 30 (1969) 2117–2134, https://doi.org/10.1016/0022-3697(69)90137-1.
[39] D.S. Jeong, H. Schroeder, R. Waser, Coexistence of bipolar and unipolar resistive switching behaviors in a Pt TiO2 Pt stack, Electrochem. Solid-State Lett. 10 (2007) 1–4, https://doi.org/10.1149/1.2742989.
[40] B. Roh, D.D. Macdonald, Effect of oxygen vacancies in anodic titanium oxide films on the kinetics of the oxygen electrode reaction, Russ. J. Electrochem. 43 (2007) 125–135, https://doi.org/10.1134/S1023193507020012.
[41] D.J. Blackwood, L.M. Peter, D.E. Williams, Stability and open circuit breakdown of the passive oxide film on titanium, Electrochim. Acta 33 (1988) 1143–1149, https://doi.org/10.1016/0013-4686(88)80206-8.
[42] L. Zhang, S. Cosemans, D.J. Wouters, G. Groeseneken, M. Jurczak, B. Govoreanu, On the optimal ON/OFF resistance ratio for resistive switching element in one-selector one-resistor crosspoint arrays, IEEE Electron Device Lett. 36 (2015) 570–572, https://doi.org/10.1109/LED.2015.2427313.

[43] D.J. Wouters, R. Waser, M. Wuttig, Phase-Change and Redox-Based Resistive Switching Memories, 103 (2015). https://doi.org/10.1109/JPROC.2015.2433311.
[44] Y. Yang, P. Sheridan, W. Lu, Complementary resistive switching in tantalum oxide-based resistive memory devices, Appl. Phys. Lett. 100 (2012), https://doi.org/10.1063/1.4719198.
[45] Q. Lu, P. Skeldon, G.E. Thompson, D. Masheder, H. Habazaki, K. Shimizu, Transport numbers of metal and oxygen species in anodic tantala, Corros. Sci. 46 (2004) 2817–2824, https://doi.org/10.1016/j.corsci.2004.03.021.
[46] D.A. Vermilyea, The kinetics of formation and structure on tantalum, Acta Metall. 1 (3) (1953) 282–294, https://doi.org/10.1016/0001-6160(53)90101-1.
[47] J.P. Kollender, A.I. Mardare, A.W. Hassel, In-situ monitoring of metal dissolution during anodization of tantalum, J. Electrochem. Soc. 164 (2017) C598–C601, https://doi.org/10.1149/2.1471709jes.
[48] A.I. Mardare, A. Ludwig, A. Savan, A.D. Wieck, A.W. Hassel, Combinatorial investigation of Hf-Ta thin films and their anodic oxides, Electrochim. Acta 55 (2010) 7884–7891, https://doi.org/10.1016/j.electacta.2010.03.066.
[49] E.M. Patrito, V.A. Macagno, C. Quimicas, Characterization of hafnium anodic oxide films: an AC impedance investigation, 40 (1995) 809–815. https://doi.org/10.1016/0013-4686(95)00003-W.
[50] G.S. Kim, T.H. Park, H.J. Kim, T.J. Ha, W.Y. Park, S.G. Kim, C.S. Hwang, Investigation of the retention performance of an ultra-thin HfO2 resistance switching layer in an integrated memory device, J. Appl. Phys. 124 (2018), https://doi.org/10.1063/1.5033967.
[51] U. Russo, D. Kamalanathan, D. Ielmini, A.L. Lacaita, M.N. Kozicki, Study of multilevel programming in Programmable Metallization Cell (PMC) memory, IEEE Trans. Electron Devices 56 (2009) 1040–1047, https://doi.org/10.1109/TED.2009.2016019.
[52] S. Menzel, U. Böttger, R. Waser, Simulation of multilevel switching in electrochemical metallization memory cells, J. Appl. Phys. 111 (2012), https://doi.org/10.1063/1.3673239.
[53] B. Pal, S. Yang, S. Ramesh, V. Thangadurai, R. Jose, Electrolyte selection for supercapacitive devices: a critical review, Nanoscale Adv. 1 (2019) 3807–3835, https://doi.org/10.1039/c9na00374f.
[54] J. Strobel, K.K. Neelisetty, V.S.K. Chakravadhanula, L. Kienle, Transmission electron microscopy on memristive devices: an overview, Appl. Microsc. 46 (2016) 206–216, https://doi.org/10.9729/am.2016.46.4.206.
[55] I. Zrinski, C.C. Mardare, L.I. Jinga, J.P. Kollender, G. Socol, A. Minenkov, A. W. Hassel, A.I. Mardare, Electrolyte-dependent modification of resistive switching in anodic hafnia, Nanomaterials 11 (2021) 1–18, https://doi.org/10.3390/nano11030666.
[56] K. Persson, The Materials Project. Materials Data on Pt by Materials Project, (n.d.). https://doi.org/10.17188/1189002.
[57] B. Mohammad, M.A. Jaoude, V. Kumar, D.M. Al Homouz, H.A. Nahla, M. Al-Qutayri, N. Christoforou, State of the art of metal oxide memristor devices, Nanotechnol. Rev. 5 (2016) 311–329, https://doi.org/10.1515/ntrev-2015-0029.